J. Fluid Mech. (2009), *vol.* 626, *pp.* 307–332. © 2009 Cambridge University Press
doi:10.1017/S0022112009005977 Printed in the United Kingdom

Motion planning and trajectory tracking for three-dimensional Poiseuille flow

JENNIE COCHRAN† AND MIROSLAV KRSTIC

Department of Mechanical and Aerospace Engineering, University of California, San Diego, La Jolla, CA 92093, USA

(Received 2 December 2007 and in revised form 19 September 2008)

We present the first solution to a boundary motion planning problem for the Navier–Stokes equations, linearized around the parabolic equilibrium in a three-dimensional channel flow. The pressure and skin friction at one wall are chosen as the reference outputs as they are the most readily measurable 'wall-restricted' quantities in experimental fluid dynamics and also because they play a special role as performance metrics in aerodynamics. The reference velocity input is applied at the opposite wall. We find the exact (method independent) solution to the motion planning problem using the PDE (partial differential equation) backstepping theory. The motion planning solution results in open-loop controls, which produce the reference output trajectories only under special initial conditions for the flow velocity field. To achieve convergence to the reference trajectory from other (nearby) initial conditions, we design a feedback controller. We also present a detailed examination of the closed-form solutions for gains and the behaviour of the motion planning solution as the wavenumbers grow or the Reynolds number grows. Numerical results are shown for the motion planning problem.

1. Introduction

What is motion planning? Motion planning, or trajectory generation, is not a common concept in fluid dynamics. However, it is a central subject in another area of mechanics – robotics. By motion planning we are referring to the following problem. Suppose one is interested in producing a particular spatio-temporal waveform on a flow boundary for some specific flow variables. Such variables may be skin friction and pressure, which are linked to aerodynamic quantities of interest such as forces and moments exerted on an aerial vehicle. These boundary flow variables are referred to as *output* variables, and their desired profile is referred to as the *reference output*. Now suppose a part of the flow boundary is instrumented with actuators such as velocity actuators. The actuated quantities, in this case the velocities at the boundary, are referred to as the flow *inputs* and their evolution over time is likewise called the *reference input*. Motion planning is defined as the problem of determining the spatio-temporal functions governing the reference inputs that generate the reference output. In our example this means determining how to actuate the velocities at the flow boundary to enforce specific skin friction and pressure output profiles. To find the functions that govern the flow input, one must first find the unique functions that govern the entire velocity field. This solution is referred to as the *state reference*

† E-mail address for correspondence: cochran.jennie@gmail.com

https://doi.org/10.1017/S0022112009005977 Published online by Cambridge University Press

trajectory as it defines the trajectory (for all space and time) that the system states (the velocity field) must take in order to satisfy the system equations and the reference output. The input/output pair for the Navier–Stokes system we consider in this paper is 'differentially flat', i.e. the reference input can be found as a functional of the reference output. This is so because the partial differential equation (PDE) problem in question is of Cauchy/Kowalevski type when the roles of t and y are exchanged. The solution can be expressed as a formal power series in y, with coefficients defined through recurrence relations based on the reference output. When the series converges, the solution is unique. Though we pursue a linearized case in this paper, flatness, as a structural property, also holds in the case of the nonlinear Navier–Stokes system and constitutes a fundamental reason why the solution we present exists and is unique. From this solution one finds the reference input.

The solution of a motion planning problem formulated in this way could be used to produce the exact temporal profiles of forces and moments acting on an aerial vehicle, using flow actuators (rather than moving flaps). Such capability is of interest for achieving low radar detectability of aircraft, but it is of just as much interest in its own right, as a fundamental problem in fluid mechanics and control theory.

As the solution to the motion planning problem is defined for all time, at the specific time $t = 0$, the velocity field needs to have a particular spatial profile in order for the reference input to produce the reference output. This is almost never going to be the case, as the initial velocity cannot be chosen by the designer, it is given. For this reason, the *open-loop* reference inputs designed to solve the motion planning problem cannot be used alone. The reference trajectory of the system state needs to be stabilized by adding a *feedback* component to the (open-loop) reference input. The design of the feedback component of the controller is referred to as *trajectory tracking*.

The two problems, motion planning design and trajectory tracking design, are independent. The solution to the former is a function (vector-valued) of time and of the spatial coordinates, whereas the solution to the latter is a function of the spatial coordinates only. This function is referred to as a *gain function* and multiplies the (time-dependent) velocity field in the feedback law. Even for *linearized* Navier–Stokes equations (around an equilibrium profile), and even for a simple geometry as the channel flow, motion planning and trajectory tracking are extremely challenging problems. Since the objective in the motion planning problem is exact, its solution is unique – and thus method independent – whereas the solution to the trajectory tracking problem is not unique and thus is method dependent. This paper presents motion planning and trajectory tracking designs for skin friction and pressure at the wall opposite to the actuated wall.

Relation to flow control for stabilization. Most of the research on model-based flow control so far has been on problems of stabilization type. The channel flow geometry has occupied a special place in this research. The work on feedback design for turbulence suppression in channel flow by boundary control was initiated with the papers by Joshi, Speyer & Kim (1997) and Bewley & Liu (1998), which employed linear quadratic optimal control techniques, and was followed by the work by Balogh, Liu & Krstic (2001) and Aamo & Krstic (2002), which employed Lyapunov techniques. This topic continues to enjoy interest, as reflected through the steady improvement of the available results Baker & Christofides (2002); Baramov, Tutty & Rogers (2002); Barbu (2003); Hogberg, Bewley & Henningson (2003); Veres *et al.* (2003); Baramov, Tutty & Rogers (2004); Raymond (2006); Ilak & Rowley (2007); Vazquez & Krstic (2007*a*, *b*). In parallel, stabilization problems in other (non-channel) geometries are

https://doi.org/10.1017/S0022112009005977 Published online by Cambridge University Press

being pursued, such as, for example, in Gunzburger & Lee (1991), Protas & Styczek (2002), Aamo & Krstic (2004) and Yuan, Krstic & Bewley (2004).

Designs for stabilization are of 'feedback' type and do not solve the main problem that we consider here – the motion planning problem. Motion planning, though new for Navier–Stokes systems, has already been considered for more accessible types of systems modelled by PDEs, particularly those of parabolic type studied by Laroche & Martin (2000), Laroche, Martin & Rouchon (2000), Ollivier & Sedoglavic (2001), Rouchon (2001) and Meurer & Zeitz (2005). While this paper presents the first solution for motion planning for a broad family of time-varying trajectories at the boundary of the channel flow system, Vazquez, Coron & Trelat (2006*a*) solve the problem of moving the system from rest to a given Poiseuille profile (equilibrium-to-equilibrium transfer).

The 'backstepping' approach. The approach that we consider here is generally referred to as 'backstepping for PDEs' and it was introduced for one-dimensional parabolic PDEs in the work by Smyshlyaev & Krstic (2004). In the work by Vazquez & Krstic (2007*a*, *b*) this method was extended to linearized Navier–Stokes equations, at arbitrary Reynolds numbers, which we use as a starting point for our efforts in developing motion planning. Backstepping is an approach that employs a particular form of a Volterra transformation in the spatial variable(s) and in a boundary control law. The combination of the transformation and the boundary control allows one to transform the system being controlled, which is typically complex, into a simple 'target' system. The basic heat equation PDE is often employed as the target system. By employing the backstepping approach, we reduce the motion planning problem for the three-dimensional Navier–Stokes channel problem to a motion planning problem for two one-dimensional heat equations. In this way, backstepping finds the unique solution to the motion planning problem. Backstepping is also employed to solve the trajectory tracking problem.

Organization of the paper. We start by reviewing the three-dimensional channel flow linearized model and giving an informal argument explaining why the solution to the motion planning problem is unique in § 2. We then state and prove the solution to the motion planning problem in § 3. The solution relies on several changes of variable, including the two-dimensional Fourier transform, the change to normal velocity and vorticity for variables and, most importantly, the PDE backstepping transformations. The successful simulation of the system forced by a given reference trajectory is also shown. A control law which stabilizes the system around the desired trajectory is introduced and discussed in § 4. We then go on to look more closely at particular closed-form solutions in § 5 and then the behaviour of the solution as the wavenumbers grow or Reynolds number grows in § 6. Specifically, the decay in the norm of the solution is shown for a specific reference trajectory. We conclude in § 7.

2. System model

We consider the three-dimensional channel flow that is infinite in the x- and z-directions and bounded by walls at $y = 0$ and $y = 1$ as seen in figure 1. The governing equations for the dimensionless velocity field of the incompressible channel flow are the Navier–Stokes equations

$$\boldsymbol{U}_t = \frac{1}{Re}\triangle \boldsymbol{U} - \boldsymbol{U}\cdot\nabla\boldsymbol{U} - \nabla P, \tag{2.1}$$

$$\nabla\cdot\boldsymbol{U} = 0, \tag{2.2}$$

https://doi.org/10.1017/S0022112009005977 Published online by Cambridge University Press

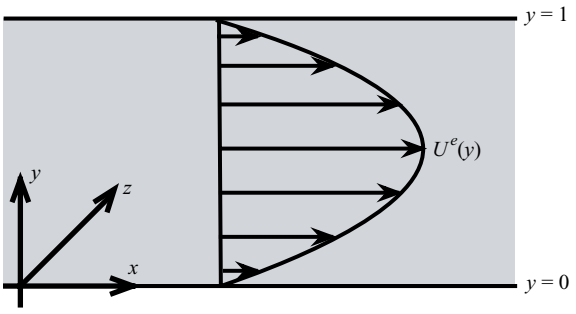


FIGURE 1. Three-dimensional channel flow.

where $\boldsymbol{U} = (U, W, V)$ and $U(y, x, z, t)$ is the streamwise velocity, $W(y, x, z, t)$ is the spanwise velocity, $V(y, x, z, t)$ is the wall-normal velocity, $P(y, x, z, t)$ is the pressure and Re is the Reynolds number. The velocities at far wall $y = 0$ satisfy the standard no-slip no-penetration boundary condition,

$$\boldsymbol{U}|_{y=0} = 0. \tag{2.3}$$

These equations are linearized around the equilibrium parabolic Poiseuille profile

$$U^e = 4y(1 - y) \tag{2.4}$$

$$W^e = V^e = 0 \tag{2.5}$$

$$P^e = P_0 - \frac{8}{Re}x. \tag{2.6}$$

After defining the fluctuation variables

$$u = U - U^e, \quad p = P - P^e, \tag{2.7}$$

the linearized system is

$$u_t = \frac{1}{Re}\triangle u - U^e u_x - U^e_y V - p_x \tag{2.8}$$

$$W_t = \frac{1}{Re}\triangle W - U^e W_x - p_z \tag{2.9}$$

$$V_t = \frac{1}{Re}\triangle V - U^e V_x - p_y \tag{2.10}$$

$$u_x + V_y + W_z = 0 \tag{2.11}$$

$$u|_{y=0} = 0 \qquad W|_{y=0} = 0 \qquad V|_{y=0} = 0. \tag{2.12}$$

The Dirichlet conditions at the far wall $y = 0$ satisfy the standard no-slip and no-penetration boundary conditions. However, the Neumann boundary variables at the same wall are used as the *reference outputs*. They are denoted by $\mathscr{Y}$ and given by the desired skin friction and pressure trajectories, $u^r_y(0, x, z, t)$, $W^r_y(0, x, z, t)$, $p^r(0, x, z, t)$. We must solve for the reference inputs, denoted by $\mathscr{U}$, and given by $u^r(1, x, z, t)$, $W^r(1, x, z, t)$, $V^r(1, x, z, t)$. These inputs are actuated at the near wall $y = 1$.

We assume all three velocities to be actuated. We stress that there is no consensus in the literature as to which velocities are physically reasonable or mathematically necessary to actuate. The possibility of both wall-normal and tangential (lateral) air injection using synthetic jets is discussed in Glezer & Allen (2002). We emphasize that

https://doi.org/10.1017/S0022112009005977 Published online by Cambridge University Press

the three velocity components at the boundary that our control laws command are neither mutually independent nor arbitrary but satisfy the Navier–Stokes PDEs.

It is important to understand what type of a mathematical problem one is facing when trying to find $\mathscr{U}$ for a given $\mathscr{Y}$. If we exchange the role of t and y, then the equations, expressed in terms of u, W, p, are

$$u_{yy} = -u_{xx} - u_{zz} + Re\left(u_t + U^e u_x + U^e_y V + p_x\right) \tag{2.13}$$

$$W_{yy} = -W_{xx} - W_{zz} + Re(W_t + U^e W_x + p_z) \tag{2.14}$$

$$p_{yy} = -p_{xx} - p_{zz} + 2U^e_y V_x. \tag{2.15}$$

Note that the left-hand side is a partial derivative of order two in y and on the right the partial derivatives with respect to t, x, z are of order two or less. Now the 'initial conditions' at $y=0$ are given by $\mathscr{Y}$, the no-slip condition ($u = W = 0$) and $p_y|_{y=0} = -1/Re(\partial/\partial x)u_y|_{y=0} - 1/Re(\partial/\partial z)W_y|_{y=0}$, (where $u_y|_{y=0}$, $W_y|_{y=0}$ are again given by $\mathscr{Y}$). Set up in this way, this is a problem of Cauchy/Kowalevski type. As such we can expand the PDE using a formal power series in y and define recurrence relations for the coefficients (as functions of the remaining independent variables). As the first and second coefficients of this series are given through the 'initial conditions', the recurrence relations define the series without any ambiguity. The normal velocity V is also defined without ambiguity through $V_y = -u_x - W_z$ and $V|_{y=0} = 0$. Therefore, if the series converges, we have a solution to u, W, V, p given $\mathscr{Y}$ and that solution is unique.

As standard for channel flow, we make use of the two-dimensional Fourier Transform in the x- and z-directions to reduce the spatial dimension of the system from three to one. It results in a continuum of one-dimensional systems, each parameterized by k_x and k_z, the wavenumbers in the x- and z-directions, respectively. As the three-dimensional PDE system is linear, each one-dimensional system is uncoupled from the others, though the subsystems within the one-dimensional system remain coupled. As the transformation between Fourier/wave space and physical space is standard, we continue the rest of the paper (unless explicitly stated) in wave space. For convenience we drop the dependence on k_x and k_z in the functions. The equations that result from the transformation are (in wave space)

$$u_t = \frac{1}{Re}\triangle_k u - 2\pi \mathrm{i} k_x U^e u - U^e_y V - 2\pi \mathrm{i} k_x p \tag{2.16}$$

$$W_t = \frac{1}{Re}\triangle_k W - 2\pi \mathrm{i} k_x U^e W - 2\pi \mathrm{i} k_z p \tag{2.17}$$

$$V_t = \frac{1}{Re}\triangle_k V - 2\pi \mathrm{i} k_x U^e V - p_y \tag{2.18}$$

$$2\pi \mathrm{i} k_x u + 2\pi \mathrm{i} k_z W + V_y = 0 \tag{2.19}$$

$$u|_{y=0} = 0 \qquad W|_{y=0} = 0 \qquad V|_{y=0} = 0, \tag{2.20}$$

where $\triangle_k = \partial^2/\partial y^2 - \alpha^2$ and $\alpha^2 = 4\pi^2(k_x^2 + k_z^2)$. The velocities $u(y,t)$, $W(y,t)$, $V(y,t)$ and pressure $p(y,t)$, as well as the reference output trajectories $u^r_y|_{y=0}$, $W^r_y|_{y=0}$, $p^r|_{y=0}$ are parameterized by the wavenumbers k_x and k_z.

https://doi.org/10.1017/S0022112009005977 Published online by Cambridge University Press

3. Motion planning

The desired reference output $\mathscr{Y} = \{u_y^r|_{y=0},\ W_y^r|_{y=0},\ p^r|_{y=0}\}$ for the skin friction and pressure is chosen within the following class of functions of (t, k_x, k_z):

$$u_y^r|_{y=0} = \sum_m A_m \mathrm{e}^{\varphi_m t}, \quad W_y^r|_{y=0} = \sum_m B_m \mathrm{e}^{\varphi_m t} \tag{3.1}$$

$$p^r|_{y=0} = \sum_m C_m \mathrm{e}^{\varphi_m t}, \tag{3.2}$$

where A_m, B_m, C_m and φ_m can all depend on the wavenumbers k_x and k_z. Indeed, φ_m can be complex – thus any sinusoid can be represented by (3.1) and (3.2).

In general these sums must be chosen such that

$$\sum_m X_m \sqrt{\frac{\epsilon}{\varphi_m}} \sinh\left(\sqrt{\frac{\varphi_m}{\epsilon}}\right) \mathrm{e}^{\varphi_m t} < \infty \qquad \forall k_x, k_z,$$

where $X_m \in \{A_m, B_m, C_m\}$. If $\varphi_m = \mathrm{i}m\varphi_0$, then X_m must be the Fourier coefficients of a function that is smooth and periodic in t. In addition the terms $X_m(k_x, k_z)$ need to decay 'fast enough' in k_x, k_z, for example, to be square integrable in k_x, k_z (where they correspond to the Fourier Transform of square integrable functions in x, z). We will discuss this in detail in § 6 where we analyse the growth of the motion planning solution.

Before stating the main result of this paper, we introduce Volterra operators and other notation. The Volterra operator is a 'spatially causal' or lower triangular change of variable which starts from the lower wall $y = 0$ and is marched forward continuously in space towards the near wall $y = 1$. This type of approach has been effective in control of finite-dimensional nonlinear systems such as robotics and flight dynamics and it is known under the names of feedback linearization (Isidori 1995), dynamic inversion and integrator backstepping (Krstic, Kanellakopoulos & Kokotovic 1995). The extension to infinite-dimensional systems was developed recently and results in explicit formulae for the gain functions Smyshlyaev & Krstic (2004). This method is based on a functional transformation $f \mapsto g$,

$$f(y) = g(y) - \int_0^y K(y, \eta) g(\eta) \mathrm{d}\eta,$$

where the second term is a Volterra integral operator with a kernel $K(y, \eta)$. This transformation is invertible and its inverse involves another Volterra operator,

$$g(y) = f(y) + \int_0^y L(y, \eta) f(\eta) \mathrm{d}\eta,$$

where the kernels $L(y, \eta)$ and $K(y, \eta)$ are related through a (non-Volterra type) integral equation

$$L(y, \eta) = K(y, \eta) + \int_\eta^y K(y, \sigma) L(\sigma, \eta) \mathrm{d}\sigma.$$

We introduce a compact Volterra operator notation as

$$\mathscr{V}(K, f)(y) = \int_0^y K(y, \eta) f(\eta) \mathrm{d}\eta,$$

where the operator output is a function of y, the upper limit of integration is the first argument of the first function and the integration is over the second argument

https://doi.org/10.1017/S0022112009005977 Published online by Cambridge University Press

of the first function and the first argument of the second function. (If the second function has more than one argument, such as time or wavenumbers, all but the first are ignored as far as the integration is concerned.) We also define

$$\mathscr{W}_{\eta}^{y}(K, L) = \int_{\eta}^{y} K(y, \sigma)L(\sigma, \eta)\mathrm{d}\sigma,$$

which is similar to $\mathscr{V}(\cdot, \cdot)$ except that (i) the lower limit of integration is the second argument of the second function and (ii) the operator output is a function of both y and η.

Next we present the main result of the paper – the full reference trajectory (for input and state), valid for all individual wavenumbers, satisfying the reference output profiles for the skin friction and pressure at the far wall (3.1) and (3.2), and consisting of a linear combination of two Volterra integrals of explicit functions with spatial gain kernels. The linear combination results from the use of the normal velocity and vorticity while the Volterra operators arise from the use of PDE backstepping theory. The solution is method independent – we simply employ backstepping to find it. Therefore, the pattern of dependence on Reynolds and wave numbers (which is examined in § 6) is not a result of the method but is inherent to the motion planning problem itself.

THEOREM 1. *The PDE system* (2.16)–(2.20) *with desired output* (3.1) *and* (3.2) *is satisfied by the following functions defined for* $(y, t) \in [0, 1] \times [0, \infty)$*:*

$$u^r = \frac{-1}{2\pi\mathrm{i}} \frac{k_x Y^r + k_z \omega^r}{k_x^2 + k_z^2} \tag{3.3}$$

$$W^r = \frac{-1}{2\pi\mathrm{i}} \frac{k_z Y^r - k_x \omega^r}{k_x^2 + k_z^2} \tag{3.4}$$

$$V^r(y, t) = \int_0^y Y^r(\eta, t)\mathrm{d}\eta \;=\; \mathscr{V}(1, Y^r), \tag{3.5}$$

where $Y^r(y, t)$ *and* $\omega^r(y, t)$ *are*

$$Y^r = \Psi^r - F + \mathscr{V}(L, \Psi^r - F) \tag{3.6}$$

$$\omega^r = \Omega^r - G + \mathscr{V}(\Phi, \Omega^r - G) + \mathscr{V}(\Theta, \Psi^r - F), \tag{3.7}$$

the functions $\Psi^r(y, t)$, $\Omega^r(y, t)$, $F(y, t)$, $G(y, t)$ *are defined by*

$$\Psi^r = -2\pi\mathrm{i} \sum_m (k_x A_m + k_z B_m)\mathrm{e}^{\varphi_m t} \sqrt{\frac{\epsilon}{\varphi_m}} \sinh\left(\sqrt{\frac{\varphi_m}{\epsilon}} y\right) \tag{3.8}$$

$$\Omega^r = -2\pi\mathrm{i} \sum_m (k_z A_m - k_x B_m)\mathrm{e}^{\varphi_m t} \sqrt{\frac{\epsilon}{\varphi_m}} \sinh\left(\sqrt{\frac{\varphi_m}{\epsilon}} y\right) \tag{3.9}$$

$$F = -\sum_m C_m \mathrm{e}^{\varphi_m t} \mathscr{V}(\sigma_m, \mathscr{V}(K, q_p) - q_P) \tag{3.10}$$

$$G = -\sum_m C_m \mathrm{e}^{\varphi_m t} \mathscr{V}(\sigma_m, \mathscr{V}(\Gamma, q_p)), \tag{3.11}$$

where $\sigma_m(y, \eta) = \sinh(\sqrt{\varphi_m/\epsilon}(y - \eta))/\sqrt{\varphi_m \epsilon}$ *and the kernels* $L(y, \eta)$, $\Theta(y, \eta)$, $\Phi(y, \eta)$, $K(y, \eta)$, $\Gamma(y, \eta)$ *are defined by the following well-posed PDEs (Smyshlyaev & Krstic 2004) in the region* $\{(y, \eta): 0 \leqslant \eta \leqslant y \leqslant 1\}$

$$\epsilon L_{yy} = \epsilon L_{\eta\eta} - \phi(y)L - f \qquad \epsilon K_{yy} = \epsilon K_{\eta\eta} + \phi(\eta)K - f$$

https://doi.org/10.1017/S0022112009005977 Published online by Cambridge University Press

$$-\mathscr{W}_{\eta}^{y}(f, L) \qquad +\mathscr{W}_{\eta}^{y}(K, f) \tag{3.12}$$

$$\epsilon L|_{\eta=y} = -\tfrac{1}{2}\mathscr{V}(1, \phi) - g(0) \qquad \epsilon K|_{\eta=y} = -\tfrac{1}{2}\mathscr{V}(1, \phi) - g(0) \tag{3.13}$$

$$\epsilon L|_{\eta=0} = -g(y) \qquad \epsilon K|_{\eta=0} = \mathscr{V}(K, g) - g(y) \tag{3.14}$$

$$\epsilon \Theta_{yy} = \epsilon \Theta_{\eta\eta} - \phi(y)\Theta - h \qquad \epsilon \Gamma_{yy} = \epsilon \Gamma_{\eta\eta} + \phi(\eta)\Gamma - h$$
$$-\mathscr{W}_{\eta}^{y}(h, L) \qquad +\mathscr{W}_{\eta}^{y}(\Gamma, f) + \mathscr{W}_{\eta}^{y}(\Pi, h) \tag{3.15}$$

$$\epsilon \Theta|_{\eta=y} = 0 \qquad \epsilon \Gamma|_{\eta=y} = 0 \tag{3.16}$$

$$\epsilon \Theta|_{\eta=0} = 0 \qquad \epsilon \Gamma|_{\eta=0} = \mathscr{V}(\Gamma, g) \tag{3.17}$$

$$\epsilon \Phi_{yy} = \epsilon \Phi_{\eta\eta} - \phi(y)\Phi \qquad \epsilon \Pi_{yy} = \epsilon \Pi_{\eta\eta} + \phi(\eta)\Pi \tag{3.18}$$

$$\epsilon \Phi|_{\eta=y} = -\tfrac{1}{2}\mathscr{V}(1, \phi) \qquad \epsilon \Pi|_{\eta=y} = -\tfrac{1}{2}\mathscr{V}(1, \phi) \tag{3.19}$$

$$\epsilon \Phi|_{\eta=0} = 0 \qquad \epsilon \Pi|_{\eta=0} = 0 \tag{3.20}$$

where

$$\epsilon = \frac{1}{Re} \tag{3.21}$$

$$\phi(y) = 8\pi \mathrm{i} k_x y(y-1) - \epsilon\alpha^2 \tag{3.22}$$

$$f(y, \eta) = 8\pi \mathrm{i} k_x (2y-1) - 32\pi \mathrm{i} \frac{k_x}{\alpha} \sinh(\alpha(y-\eta)) - 16\pi \mathrm{i} k_x (2\eta - 1)\cosh(\alpha(y-\eta)) \tag{3.23}$$

$$g(y) = -\epsilon\alpha \sinh(\alpha y) \tag{3.24}$$

$$q_P(y) = -\alpha^2 \cosh(\alpha y) \tag{3.25}$$

$$h(y, \eta) = 8\pi k_z \mathrm{i}(1-2y)\,. \tag{3.26}$$

The reference input is given by $u^r|_{y=1}$, $W^r|_{y=1}$ *and*

$$V^r|_{y=1} = \mathrm{e}^{-(\alpha^2/Re)t} \int_0^t \mathrm{e}^{(\alpha^2/Re)\tau} \left(\frac{Y_y^r|_{y=1}}{Re} - \cosh(\alpha)\frac{Y_y^r|_{y=0}}{Re} + 4\pi \mathrm{i} k_x \frac{\cosh(\alpha y)}{\sinh(\alpha)} \int_0^1 V^r(\eta, \tau) U_y^e(\eta) \cosh(\alpha(1-\eta))\mathrm{d}\eta - \alpha \sinh(\alpha) \sum_m C_m \mathrm{e}^{\varphi_m \tau} \right) \mathrm{d}\tau + \mathscr{V}(1, Y^r|_{t=0})|_{y=1}. \tag{3.27}$$

We prove Theorem 1 by construction in § 3.1 to help the reader gain insight into the design aspects and the structure of the solution. The structure of the problem is pictorially represented in figure 2. We start with the linearized Navier–Stokes equations (2.16)–(2.20) and forcing trajectories (3.1) and (3.2) and perform several transformations (shown in figure 3) to divide the problem into several tractable problems. After solving these simpler motion planning problems, we transform the solutions back to the velocity variables. The steps are summarized as follows:

(i) Solve for the pressure and find a (open loop) normal velocity controller to reduce the open-loop problem from three velocity variables and one pressure variable down to three velocity variables.

(ii) Employ a transformation that reduces the model with three velocity variables to a model with only two variables in the normal direction – the normal vorticity ω^r and the derivative of the normal velocity in the normal direction $Y^r = V_y^r$.

https://doi.org/10.1017/S0022112009005977 Published online by Cambridge University Press

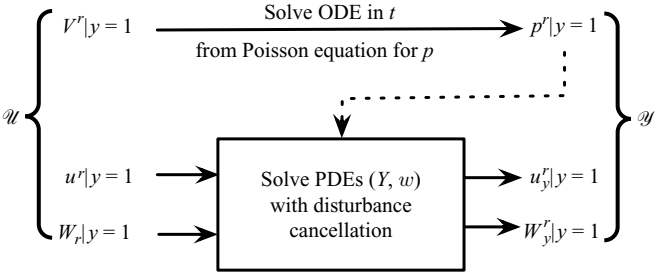


FIGURE 2. The structure of the input–output relationship $\mathscr{U} \mapsto \mathscr{Y}$ and a description of the types of problems that are solved in constructing the input $\mathscr{U}$ for a given reference output $\mathscr{Y}$. Finding $V^r|_{y=1}$ is 'easy' – it involves only a solution to an ODE in the time variable, given the pressure reference $p^r|_{y=0}$. Finding $u^r|_{y=1}$ and $W^r|_{y=1}$ is more complicated as it involves solving the Cauchy/Kowalevski problem for two coupled PDEs with a given output reference $u^r_y|_{y=0}$, $W^r_y|_{y=0}$, combined with solving an exact disturbance cancellation problem, where the pressure reference $p^r|_{y=0}$ acts as a known disturbance.

$$\{u, W, V, p\} \leftrightarrows \{Y, w\} \quad \underset{K, \prod, \Gamma}{\overset{L, \Phi, \Theta}{\Longleftrightarrow}} \quad \{\Psi - F, \Omega - G\}$$

FIGURE 3. The string of (invertible) transformations involved in solving the full-state motion planning problem.

(iii) Use the PDE backstepping transformation (employing Volterra integral operators and kernels K, Π, Γ) to transform the more complex model (Y^r, ω^r) to simple heat equations for (Ψ^r, Ω^r) and (F, G).

(iv) Solve the heat equations which define Ψ^r, Ω^r. These are forced at the boundary by $u^r_y|_{y=0}$, $W^r_y|_{y=0}$.

(v) Solve the heat equations which define F, G. These are forced internally by $p^r|_{y=0}$.

(vi) Use the inverse transformation (also employing Volterra integral operators and kernels L, Φ, Θ) to transform back from Ψ^r, Ω^r and F, G to Y^r, ω^r.

(vii) A linear combination of Y^r and ω^r gives us u^r, W^r, V^r.

3.1. *Proof of Theorem 1 and construction of open loop control*

Solve for the full pressure reference trajectory. Rather than working with four different variables (three velocity variables and one pressure variable – which is further complicated by a non-dynamic constraint), we instead use only two variables in the normal direction. Before stating the system equations for these two variables, we identify the input velocity trajectory in the normal direction $V^r|_{y=1}$ that ensures that the output pressure trajectory $p^r|_{y=0}$ is satisfied (exactly, i.e. for all time). The explicit solution to the elliptic PDE for p,

$$\begin{aligned} \triangle_k p &= -4\pi i k_x U^e_y V \\ p_y|_{y=0} &= -2\pi i \frac{k_x u_y|_{y=0} + k_z W_y|_{y=0}}{Re} \\ p_y|_{y=1} &= \frac{-2\pi i (k_x u_y|_{y=1} + k_z W_y|_{y=1}) - \alpha^2 V|_{y=1}}{Re} - V_t|_{y=1} \end{aligned}$$

https://doi.org/10.1017/S0022112009005977 Published online by Cambridge University Press

is

$$p = \frac{1}{\alpha}\Bigg\{ -4\pi i k_x \mathscr{V}(U_y^e(\eta)\sinh(\alpha(y-\eta)), V) + 4\pi i k_x \frac{\cosh(\alpha y)}{\sinh(\alpha)} \int_0^1 V(\eta,t) U_y^e(\eta)\cosh(\alpha(1-\eta))\mathrm{d}\eta - \frac{\cosh(\alpha(1-y))}{\sinh(\alpha)} \frac{(-2\pi i)(k_x u_y|_{y=0} + k_z W_y|_{y=0})}{Re} + \frac{\cosh(\alpha y)}{\sinh(\alpha)} \left(\frac{(-2\pi i)(k_x u_y|_{y=1} + k_z W_y|_{y=1}) - \alpha^2 V|_{y=1}}{Re} - V_t|_{y=1} \right) \Bigg\}. \quad (3.28)$$

By choosing the open-loop control $V^r|_{y=1} = \mathscr{N}$, where $\mathscr{N}$ verifies

$$\mathscr{N}_t = -\frac{\alpha^2}{Re}\mathscr{N} + \frac{(-2\pi i)(k_x u_y|_{y=1} + k_z W_y|_{y=1})}{Re} - \cosh(\alpha)\frac{(-2\pi i)(k_x u_y|_{y=0} + k_z W_y|_{y=0})}{Re} + 4\pi i k_x \frac{\cosh(\alpha y)}{\sinh(\alpha)} \int_0^1 V^r(\eta,t) U_y^e(\eta)\cosh(\alpha(1-\eta))\mathrm{d}\eta - \alpha\sinh(\alpha)\sum_m C_m e^{\varphi_m t}, \quad (3.29)$$

i.e. when $V^r|_{y=1}$ is defined as (3.27), we arrive at the motion planning solution for p^r:

$$p^r = \frac{1}{\alpha}\Bigg\{ -4\pi i k_x \mathscr{V}(U_y^e(\eta)\sinh(\alpha(y-\eta)), V^r) + \sinh(\alpha y)\frac{(-2\pi i)(k_x u_y|_{y=0} + k_z W_y|_{y=0})}{Re} + \alpha\cosh(\alpha y)\sum_m C_m e^{\varphi_m t} \Bigg\}, \quad (3.30)$$

where $p^r|_{y=0}$ is exactly (3.2). The control (3.29) conveniently absorbs the non-strict feedback (spatially non-causal) term – the integral from zero to one – into the normal velocity reference input, allowing for the rest of the motion planning problem (for u^r and W^r) to be approached using the backstepping method.

Reduce system to two variables in the normal direction. As is standard, we make use of the continuity equation and work with a variant of the normal velocity and the normal vorticity

$$Y^r = V_y^r = -2\pi i(k_x u^r + k_z W^r) \quad (3.31)$$

$$\omega^r = -2\pi i(k_z u^r - k_x W^r). \quad (3.32)$$

We see from a first glance at the evolution equations (where we have used the fact that V has a homogeneous Dirichlet boundary condition at $y = 0$ to inversely relate V to Y)

$$Y_t^r = \frac{1}{Re}\triangle_k Y^r - 2\pi i k_x U^e Y^r + 2\pi i k_x U_y^e \mathscr{V}(1, Y^r) - \alpha^2 p^r \quad (3.33)$$

$$\omega_t^r = \frac{1}{Re}\triangle_k \omega^r - 2\pi i k_x U^e \omega^r + 2\pi i k_z U_y^e \mathscr{V}(1, Y^r) \quad (3.34)$$

that we must solve for p^r if we wish to retain two second-order subsystems instead of the fourth-order and second-order subsystem seen in the Orr–Sommerfeld equations.

At this point we know p^r and $V^r|_{y=1}$ and may now take these into account to construct the rest of the motion planning solution. Substituting (3.30) into (3.33) the

https://doi.org/10.1017/S0022112009005977 Published online by Cambridge University Press

full 'cascade' system for the two variables Y^r, ω^r is

$$Y^r_t = \epsilon Y^r_{yy} + \phi(y) Y^r + g(y) Y^r_y|_{y=0} + \mathscr{V}(f, Y^r) + q_P(y) \sum_m C_m \mathrm{e}^{\varphi_m t} \tag{3.35}$$

$$\omega^r_t = \epsilon \omega^r_{yy} + \phi(y) \omega^r + \mathscr{V}(h, Y^r) \tag{3.36}$$

$$Y^r|_{y=0} = 0 \qquad Y^r_y|_{y=0} = -2\pi \mathrm{i} \sum_m (k_x A_m + k_z B_m) \mathrm{e}^{\varphi_m t} \tag{3.37}$$

$$\omega^r|_{y=0} = 0 \qquad \omega^r_y|_{y=0} = -2\pi \mathrm{i} \sum_m (k_z A_m - k_x B_m) \mathrm{e}^{\varphi_m t}, \tag{3.38}$$

where we use the homogeneous Neumann boundary condition for V in the boundary conditions for Y. By 'cascade' we mean that Y^r feeds into the w^r equation but not the other way around, which will be exploited in our design. Note also that the Y^r equation is forced by the pressure output trajectory.

Construct the forward PDE backstepping transformation. This step employs the PDE backstepping method. This method for finding stabilizing boundary controllers for parabolic PDE systems is introduced and explained in Smyshlyaev & Krstic (2004). In this paper, though we do use the method to find *stabilizing* controllers, its main use is in breaking up the entire *motion planning* problem into solvable steps and finding the full spatio-temporal reference trajectory. It is important to note that this solution is method independent – we simply take advantage of backstepping to find it constructively.

The backstepping method exploits the invertibility of transformations that employ a shift by a Volterra operator, which has a triangular structure. We start with the block-triangular transformation $(Y^r, \omega^r) \mapsto (\Psi^r - F, \Omega^r - G)$ given by

$$\Psi^r - F = Y^r + \mathscr{V}(K, Y^r) \tag{3.39}$$

$$\Omega^r - G = \omega^r + \mathscr{V}(\Gamma, Y^r) + \mathscr{V}(\Pi, \omega^r), \tag{3.40}$$

where Ψ^r, Ω^r and F, G are defined later. The forcing term $q_P(y) \sum_m C_m \mathrm{e}^{\varphi_m t}$ in (3.35), which comes from the pressure reference, complicates the motion planning problem for the streamwise and spanwise wall shear stress output trajectories, $u^r_y|_{y=0}$, $W^r_y|_{y=0}$. This pressure term acts as a known disturbance that needs to be cancelled by the controls $u^r|_{y=1}$, $W^r|_{y=1}$, which have a simultaneous task of also generating the output trajectory $u^r_y|_{y=0}$, $W^r_y|_{y=0}$. The (main) motion planning part of the state trajectory is (Ψ_r, Ω^r), whereas the disturbance cancellation part is (F, G). We first decide how we want Ψ^r and Ω^r to behave and from there we then define the gain kernels K, Π, Γ and find the equations that govern F, G. We set the boundary conditions of Ψ^r, Ω^r to match the boundary conditions of Y^r, ω^r and set the boundary conditions of F, G to zero. We also want the simplest parabolic PDE the method will allow to govern the behaviour of Ψ^r and Ω^r – arriving at uncoupled forced heat equations

$$\Psi^r_t = \epsilon \Psi^r_{yy} \qquad \Omega^r_t = \epsilon \Omega^r_{yy} \tag{3.41}$$

$$\Psi^r|_{y=0} = 0 \qquad \Omega^r|_{y=0} = 0 \tag{3.42}$$

$$\Psi^r_y|_{y=0} = -2\pi \mathrm{i} \sum_m (k_x A_m + k_z B_m) \mathrm{e}^{\varphi_m t} \qquad \Omega^r_y|_{y=0} = -2\pi \mathrm{i} \sum_m (k_z A_m - k_x B_m) \mathrm{e}^{\varphi_m t}. \tag{3.43}$$

The gain kernels K, π, Γ which allow the transformation (3.39) and (3.40) to decouple the cascade system (3.35)–(3.38) and transform it to the uncoupled system (3.41)–(3.43) are defined by the hyperbolic PDEs (3.12)–(3.20). These PDEs can be solved

https://doi.org/10.1017/S0022112009005977 Published online by Cambridge University Press

numerically or symbolically using an equivalent integral equation formulation that can be solved via a successive approximation series (Smyshlyaev & Krstic 2004). The procedure to find the PDEs which govern the gain kernels can be found in Krstic, Cochran & Vazquez (2008). This procedure extends easily allowing us to find the governing equations for F and G

$$F_t = \epsilon F_{yy} + (\mathscr{V}(K, q_P) - q_P(y)) \sum_m C_m e^{\varphi_m t} \tag{3.44}$$

$$G_t = \epsilon G_{yy} + \mathscr{V}(\Gamma, q_P) \sum_m C_m e^{\varphi_m t} \tag{3.45}$$

$$\begin{aligned} F_y(0) = 0,\ G_y(0) = 0 \\ F(0) = 0, \quad G(0) = 0\,. \end{aligned} \tag{3.46}$$

Solve for Ψ^r, Ω^r. The motion planning problem for Ψ^r, Ω^r defined by (3.41)–(3.43) can be solved by representing Ψ^r or Ω^r as a power series expansion in y – i.e. $\Psi^r = \sum_l^\infty a_l(t) y^l / l!$. After solving for $a_l(t)$, the resulting series can be explicitly summed as the sinh function seen in the solution (3.8) and (3.9).

Solve for F, G. The equations governing F, G can be solved by taking the Laplace transform in y and then solving the resulting first-order ordinary differential equation in t. The inverse Laplace transform results in the solution (3.10) and (3.11).

Find the inverse of the PDE backstepping transformation. After breaking the full problem down to simpler motion planning problems and a number of PDE equations governing gain kernels, we must inversely relate Ψ^r, Ω^r and F, G to Y^r, ω^r. This inverse relationship (3.6) and (3.7) also uses Volterra integrals, this time with gain kernels L, Θ, Φ. The gain kernels are defined by (3.12)–(3.20) and can be related to the forward transform gain kernels through the following integral equations:

$$\begin{aligned} L &= K + \mathscr{W}^y_\eta(K, L) \\ \Phi &= \Pi + \mathscr{W}^y_\eta(\Pi, \Phi) \\ \Theta &= \Gamma + \mathscr{W}^y_\eta(\Gamma, L) + \mathscr{W}^y_\eta(\Pi, \Theta). \end{aligned}$$

Retrieve u^r, W^r, V^r. The two velocity variables u^r, W^r are recovered through the linear combinations of the two variables Y^r, ω^r (3.3) and (3.4), while V^r is recovered as the integral of Y^r (3.5).

3.2. *Simulation results on motion planning*

We illustrate the motion planning solution that results when choosing a specific spatio-temporal waveform for the skin friction and pressure at the far wall (a reference output trajectory) and applying the techniques presented in this paper to obtain the exact initial conditions plus the exact input velocity (reference input) trajectories at the near wall. The figures show motion planning results for the following spatio-temporal output reference trajectory

$$u^r_y|_{y=0} = \begin{cases} e^{-(16\pi^2/25)(k_x^2/100 + k_z^2/9)} \sin((4\pi k_x + 1/2)t), & k_z \geqslant 0 \\ 0, & k_z < 0 \end{cases} \tag{3.47}$$

$$W^r_y|_{y=0} = \begin{cases} e^{-(32\pi^2/25)(k_x^2/100 + k_z^2/9)} i \sin((4\pi k_x + 1/2)t), & k_z \geqslant 0 \\ 0, & k_z < 0 \end{cases} \tag{3.48}$$

$$p^r|_{y=0} = \begin{cases} 4\pi\left(i\frac{k_x}{10} + \frac{k_z}{3}\right) e^{-(32\pi^2/25)(k_x^2/100 + k_z^2/9)} \sin((4\pi k_x + 1/2)t), & k_z \geqslant 0 \\ 0, & k_z < 0 \end{cases} \tag{3.49}$$

https://doi.org/10.1017/S0022112009005977 Published online by Cambridge University Press

written in wavespace. We emphasize that the figures show the exact solution and include no feedback component – in other words, we did not simulate the linearized Navier–Stokes equations, instead we computed the solution (3.3)–(3.5).

To show the general applicability of the method towards possibly complex problems, the output reference trajectory (3.47)–(3.49) is chosen as more complex than any particular physical application that we can think of would call for.

Figures 4 and 5 show snapshots in time of the spatio-temporal profile (3.47)–(3.49) in physical space. The arrows in figure 4 indicate the direction and magnitude of the output skin friction at the far wall $y=0$. The colours in figure 5 indicate the output pressure at $y=0$ with blue being low pressure and red being high pressure. Time proceeds left to right and top to bottom in all figures.

Figures 6 and 7 result from applying the solution at $Re=20$ to the above profile. The figures show snapshots in time of the exact input velocities that must be actuated at the near wall $y=1$ to obtain the trajectories seen in figures 4 and 5. The arrows in figure 6 indicate the direction and magnitude of the (u^r, W^r) reference input velocity vector. The colours in figure 7 represent the value of the normal velocity reference input with blue denoting negative velocities and red denoting positive velocities.

4. Stabilization

As one cannot choose the initial conditions of the flow, we must look to the addition of a feedback component to the reference input. Towards this end, we present a feedback law that accomplishes the stabilization of the linearized Navier–Stokes system about the trajectory (3.3)–(3.5). Similarly to the motion planning solution, the feedback law is derived using the PDE backstepping method. However, unlike the motion planning solution which is unique, the choice of a stabilizing feedback is not. While previous optimal control designs required actuation of only the normal or only the tangential components of velocity, but at both walls, our approach employs actuation of all three velocity components but only at the far wall $y=1$. One of the advantages of the backstepping approach over optimal control approaches, when applied to the channel flow, is that it is not necessary to solve high-dimensional Riccati equations, and the backstepping gains (the kernels) are explicit (symbolically computable) functions of the Reynolds number and the wavenumbers. Though the feedback law that we present here employs full state feedback, an observer developed in Vazquez, Schuster & Krstic (2006*b*) allows us to implement the controller by measuring only the pressure and the skin friction at the same wall as the output reference $y=0$.

THEOREM 2. *The feedback boundary controller, actuating the three velocities at the near wall* $y=1$,

$$u|_{y=1} = \sum_m A_m \mathrm{e}^{\varphi_m t} \sqrt{\frac{\epsilon}{\varphi_m}} \sinh\left(\sqrt{\frac{\varphi_m}{\epsilon}}\right) + \mathscr{V}\left(\frac{k_x^2 K + k_z^2 \Pi + k_z k_x \Gamma}{k_x^2 + k_z^2}, u\right)\Big|_{y=1}$$
$$+\mathscr{V}\left(\frac{k_x k_z K - k_z k_x \Pi + k_z^2 \Gamma}{k_x^2 + k_z^2}, W\right)\Big|_{y=1} - \frac{1}{2\Pi \mathrm{i}} \frac{k_x F|_{y=1} + k_z G|_{y=1}}{k_x^2 + k_z^2} \tag{4.1}$$

$$W|_{y=1} = \sum_m B_m \mathrm{e}^{\varphi_m t} \sqrt{\frac{\epsilon}{\varphi_m}} \sinh\left(\sqrt{\frac{\varphi_m}{\epsilon}}\right) + \mathscr{V}\left(\frac{k_z k_x K - k_x k_z \Pi - k_x^2 \Gamma}{k_x^2 + k_z^2}, u\right)\Big|_{y=1}$$
$$+\mathscr{V}\left(\frac{k_z^2 K + k_x^2 \Pi - k_x k_z \Gamma}{k_x^2 + k_z^2}, W\right)\Big|_{y=1} - \frac{1}{2\pi \mathrm{i}} \frac{k_z F|_{y=1} - k_x G|_{y=1}}{k_x^2 + k_z^2} \tag{4.2}$$

https://doi.org/10.1017/S0022112009005977 Published online by Cambridge University Press

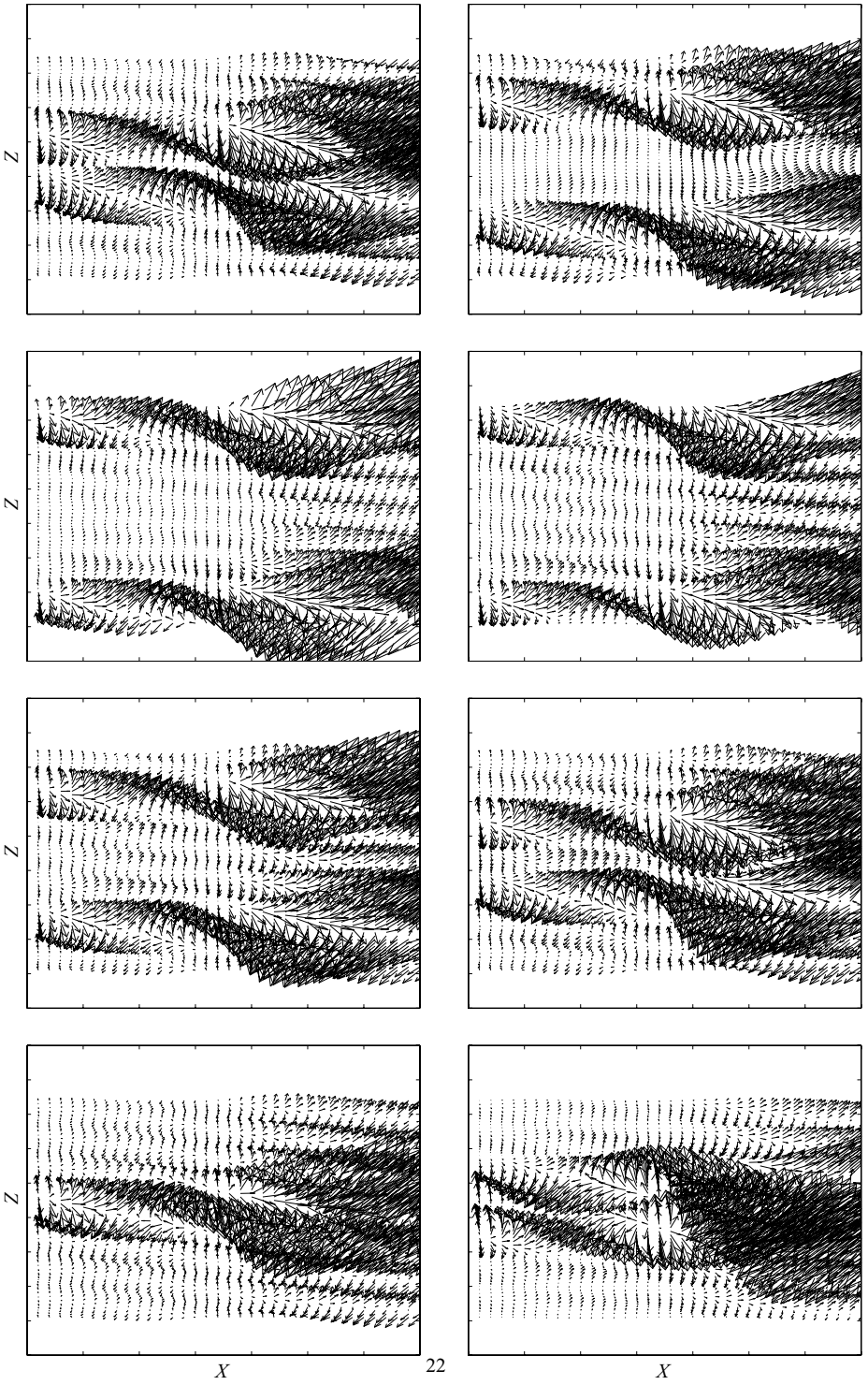


FIGURE 4. Snapshots of the desired skin friction spatio-temporal profile (reference output trajectory). Time proceeds left to right and top to bottom. Arrows indicate direction and magnitude.

https://doi.org/10.1017/S0022112009005977 Published online by Cambridge University Press

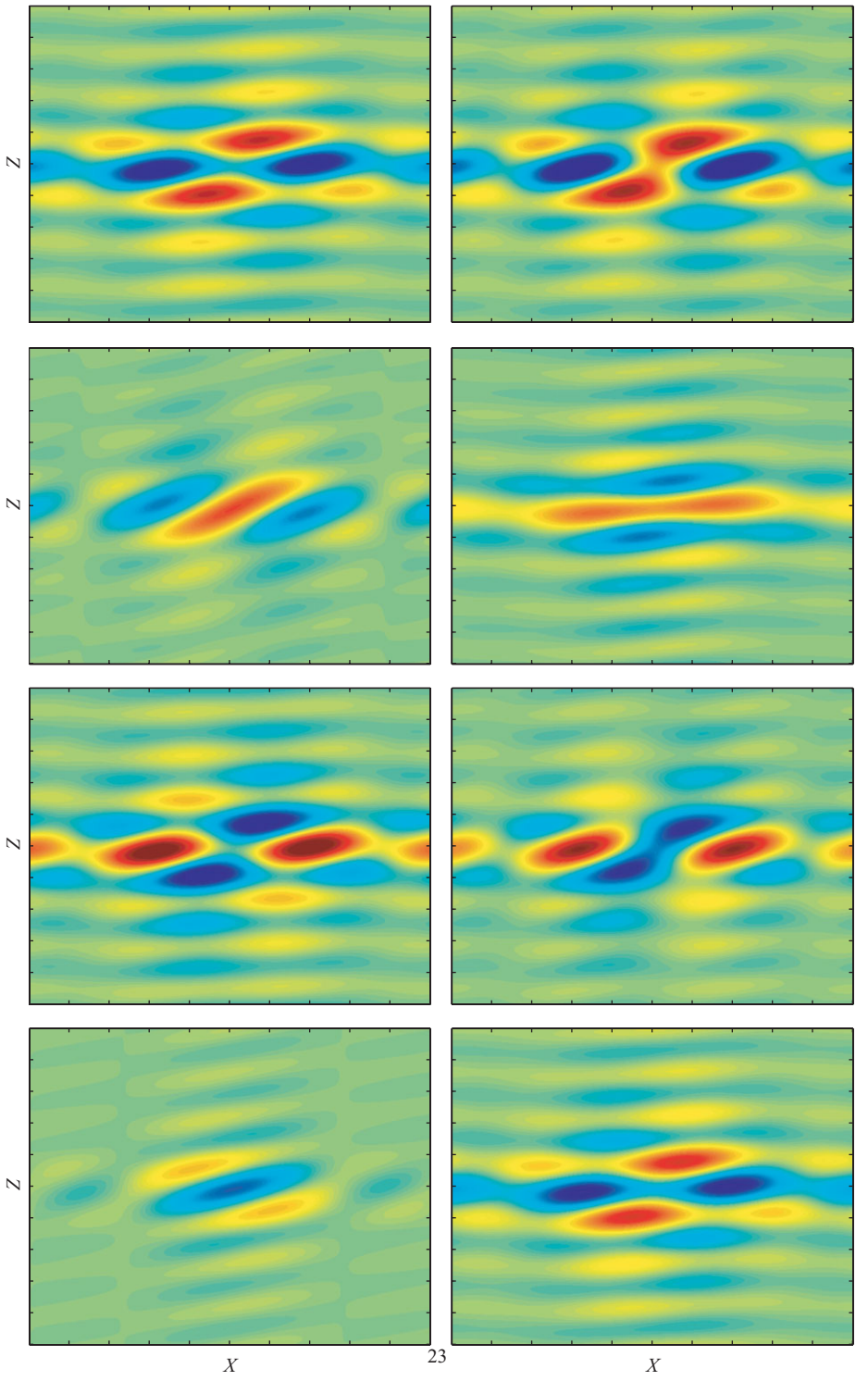


FIGURE 5. Snapshots of the desired pressure spatio-temporal profile (reference output trajectory). Time proceeds left to right and top to bottom. Blue indicates low pressure while red indicates high pressure.

https://doi.org/10.1017/S0022112009005977 Published online by Cambridge University Press

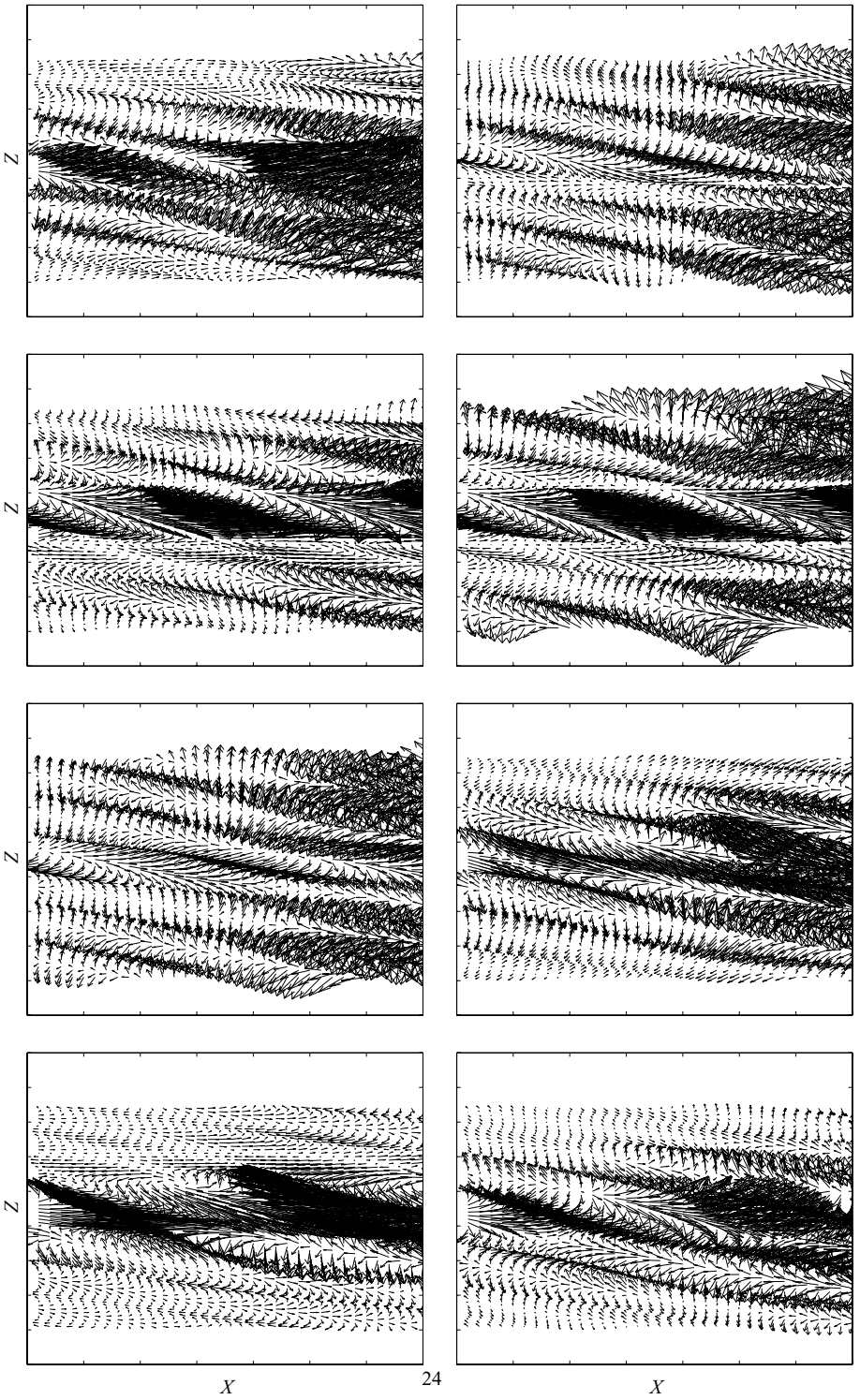


FIGURE 6. Snapshots in time of the input reference trajectory for streamwise and spanwise velocities. Time proceeds left to right and top to bottom. Arrows indicate direction and magnitude.

https://doi.org/10.1017/S0022112009005977 Published online by Cambridge University Press

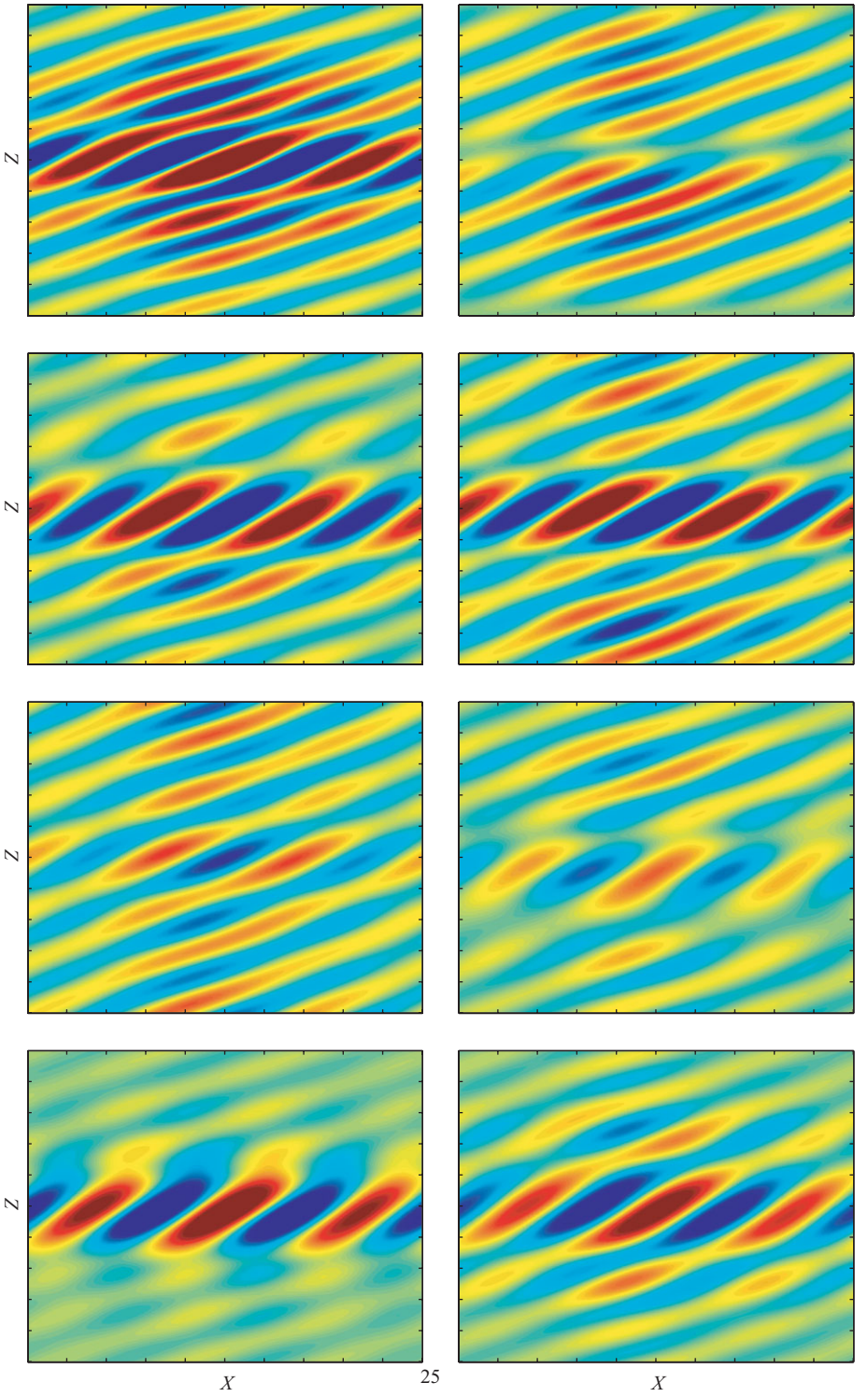


FIGURE 7. Snapshots in time of the input reference trajectory for normal velocity. Time proceeds left to right and top to bottom. Blue indicates negative velocity while red indicates positive velocity.

https://doi.org/10.1017/S0022112009005977 Published online by Cambridge University Press

$$V(t,1)_t = \mathrm{e}^{-(\alpha^2/Re)t}\int_0^t \mathrm{e}^{(\alpha^2/Re)\tau}\left(\frac{2\pi \mathrm{i}}{Re}(\cosh(\alpha)(k_x u_y|_{y=0} + k_z W_y|_{y=0}) - (k_x u_y|_{y=1} + k_z W_y|_{y=1})) + 4\pi \mathrm{i} k_x \frac{\cosh(\alpha y)}{\sinh(\alpha)}\int_0^1 V(\eta,\tau)U_y^e(\eta)\cosh\big(\alpha(1-\eta)\big)\mathrm{d}\eta - \alpha\sinh(\alpha)\sum_m C_m \mathrm{e}^{\varphi_m \tau}\right)\mathrm{d}\tau \tag{4.3}$$

exponentially stabilizes the system (2.16)–(2.20) *about the solution* (3.3)–(3.5) *in the* L_2 *sense*

$$\int_0^1 (|u-u^r|^2 + |W-W^r|^2 + |V-V^r|^2)\mathrm{d}y \leqslant C\mathrm{e}^{-\epsilon t}\int_0^1 (|u|_{t=0} - u^r|_{t=0}|^2 + |W|_{t=0} - W^r|_{t=0}|^2 + |V|_{t=0} - V^r|_{t=0}|^2)\mathrm{d}y, \tag{4.4}$$

where $\epsilon = 1/Re$ *and*

$$\begin{aligned} C &= (1+\alpha^2)(1+||L||_\infty)^2(1+||K||_\infty)^2 \\ &\quad \times ((1+||\Phi||_\infty)^2 + ||\Theta||_\infty(1+||\Phi||_\infty + ||\Theta||_\infty)) \\ &\quad \times ((1+||\Pi||_\infty)^2 + ||\Gamma||_\infty(1+||\Pi||_\infty + ||\Gamma||_\infty)) \end{aligned} \tag{4.5}$$

$$||\cdot||_\infty = \sup_{0\leqslant\eta\leqslant y\leqslant 1}\{\cdot\}. \tag{4.6}$$

Proof. To prove stability about the solution (3.3)–(3.5), we first note that the pressure is still defined by (3.28) and becomes (3.30) when the normal velocity component of the feedback is defined as in (4.3). We then write the system in terms of Y and ω. The error system ($\tilde{Y} = Y - Y^r$, $\tilde{\omega} = \omega - \omega^r$) then has the following dynamics:

$$\tilde{Y}_t = \epsilon\tilde{Y}_{yy} + \phi(y)\tilde{Y} + g(y)\tilde{Y}_y(0) + \mathscr{V}(f,\tilde{Y}) \tag{4.7}$$

$$\tilde{\omega}_t = \epsilon\tilde{\omega}_{yy} + \phi(y)\tilde{\omega} + \mathscr{V}(h,\tilde{Y}) \tag{4.8}$$

$$\tilde{Y}|_{y=1} = \mathscr{V}(K,\tilde{Y})|_{y=1} \tag{4.9}$$

$$\tilde{\omega}|_{y=1} = \mathscr{V}(\Pi,\tilde{\omega})|_{y=1} + \mathscr{V}(\Gamma,\tilde{Y})|_{y=1} \tag{4.10}$$

$$\tilde{Y}|_{y=0} = 0 \qquad \tilde{\omega}|_{y=0} = 0 \tag{4.11}$$

where we made use of (3.39) and (3.40) to determine the value of the $Y^r|_{y=1}, \omega^r|_{y=1}$. Using the standard backstepping transformation

$$\tilde{\Psi} = \tilde{Y} - \mathscr{V}(K,\tilde{Y}) \tag{4.12}$$

$$\tilde{\Omega} = \tilde{\omega} - \mathscr{V}(\Pi,\tilde{\omega}) - \mathscr{V}(\Gamma,\tilde{Y}), \tag{4.13}$$

where $K(y,\eta)$, $\Pi(y,\eta)$, $\Gamma(y,\eta)$ are still defined by (3.12)–(3.20), we arrive at the dynamics for the backstepping error variables

$$\begin{aligned} \tilde{\Psi}_t &= \epsilon\tilde{\Psi}_{yy} & \tilde{\Omega}_t &= \epsilon\tilde{\Omega}_{yy} \\ \tilde{\Psi}|_{y=0} &= 0 & \tilde{\Omega}|_{y=0} &= 0 \\ \tilde{\Psi}|_{y=1} &= 0 & \tilde{\Omega}|_{y=1} &= 0 \end{aligned} \tag{4.14}$$

which are uncoupled heat equations. The use of the backstepping transformation (4.12) and (4.13) shifts the coupling effects of the cascade system (4.7)–(4.11) to the boundary.

https://doi.org/10.1017/S0022112009005977 Published online by Cambridge University Press

These coupling effects (related to the non-normality of the Orr–Sommerfeld–Squire operator) cause small time algebraic growth in the Squire equation. To deal with this, the boundary control law cancels them. The variables $\tilde{\Psi}$ and $\tilde{\Omega}$ can be bounded as follows:

$$\int_0^1 |\tilde{\Psi}|^2 \mathrm{d}y \leqslant \mathrm{e}^{-\epsilon t} \int_0^1 |\tilde{\Psi}|_{t=0}|^2 \mathrm{d}y \tag{4.15}$$

$$\int_0^1 |\tilde{\Omega}|^2 \mathrm{d}y \leqslant \mathrm{e}^{-\epsilon t} \int_0^1 |\tilde{\Omega}|_{t=0}|^2 \mathrm{d}y. \tag{4.16}$$

Thus, we can bound the L_2 norm of the error system as in (4.4) by using the forward and inverse transformations (3.6) and (3.7) and (3.39) and (3.40). □

Note that this controller and stability theorem are defined for any wavenumber though the control is not actually meant to be applied for high wavenumbers as the inverse Fourier Transform would not converge in that case. When using this control law to stabilize the reference solution, the functions $A_m(k_x, k_z)$, $B_m(k_x, k_z)$, $C_m(k_x, k_z)$ should have compact (though arbitrarily large) support set $\mathscr{S}$ in (k_x, k_z), whereas the control law (4.1)–(4.3) should be applied for a sufficiently large disc $\mathscr{D}$ (around the origin) in wavenumber space (k_x, k_z), where $\mathscr{S} \subset \mathscr{D}$. The controller (4.1)–(4.3) can be written either as a function of time plus a function of state (as it is now), or, as a function of time plus a function of the tracking error (the tilde variables). In the latter form, one can truncate the feedback gains as low as permitted to still have stability. This truncation would not change the perfect tracking ability of the control law but it would lead to a slower decay of the tracking error to zero. The uncontrolled wavenumber set $\mathrm{Re}^2 \backslash \mathscr{D}$ takes advantage of the stability of these (truncated) wavenumber pairs around a zero velocity profile. Details about this can be found in Krstic *et al.* (2008).

5. Closed-form solutions to the kernel PDEs

The kernel PDEs (3.12)–(3.20) can be solved numerically, by using a modified Ablowitz–Kruskal–Ladik scheme (Ablowitz, Kruskal & Ladik 1979), or symbolically, by using the method of successive approximations (Smyshlyaev & Krstic 2004). In certain cases we can find the solutions in closed form. Setting the streamwise wavenumber k_x to zero is one such case. In terms of control of channel flow turbulence, this is an important scenario as it is the case where the transient growth is the largest (Bamieh & Dahleh 2001; Bewley 2001; Schmid & Henningson 2001; Jovanovic & Bamieh 2005), thus it is of interest that we can find closed-form solutions for this case.

THEOREM 3. *The PDE systems*

$$\epsilon L_{yy} = \epsilon L_{\eta\eta} + \epsilon\kappa^2 L \qquad \epsilon K_{yy} = \epsilon K_{\eta\eta} - \epsilon\kappa^2 K \tag{5.1}$$

$$\epsilon L|_{\eta=0} = -g(y) \qquad \epsilon K|_{\eta=0} = \mathscr{V}(K, g) - g(y) \tag{5.2}$$

$$\epsilon L|_{\eta=y} = \epsilon\frac{\kappa^2 y}{2} \qquad \epsilon K|_{\eta=y} = \epsilon\frac{\kappa^2 y}{2} \tag{5.3}$$

$$\epsilon \Theta_{yy} = \epsilon\Theta_{\eta\eta} + \epsilon\kappa^2\Theta - h - \mathscr{W}^y_\eta(h, L) \qquad \epsilon \Gamma_{yy} = \epsilon\Gamma_{\eta\eta} - \epsilon\kappa^2\Gamma - h + \mathscr{W}^y_\eta(\Pi, h) \tag{5.4}$$

$$\epsilon\Theta|_{\eta=0} = 0 \qquad \epsilon\Gamma|_{\eta=0} = \mathscr{V}(\Gamma, g) \tag{5.5}$$

$$\epsilon\Theta|_{\eta=y} = 0 \qquad \epsilon\Gamma|_{\eta=y} = 0 \tag{5.6}$$

https://doi.org/10.1017/S0022112009005977 Published online by Cambridge University Press

$$\epsilon \Phi_{yy} = \epsilon \Phi_{\eta\eta} + \epsilon \kappa^2 \Phi \qquad \epsilon \Pi_{yy} = \epsilon \Pi_{\eta\eta} - \epsilon \kappa^2 \Pi \tag{5.7}$$

$$\epsilon \Phi|_{\eta=0} = 0 \qquad \epsilon \Pi|_{\eta=0} = 0 \tag{5.8}$$

$$\epsilon \Phi|_{\eta=y} = \epsilon \frac{\kappa^2 y}{2} \qquad \epsilon \Pi|_{\eta=y} = \epsilon \frac{\kappa^2 y}{2} \tag{5.9}$$

are satisfied by the functions

$$L = \kappa \sinh(\kappa(y-\eta)) + \Phi + \mathscr{W}_{\eta}^{y}(\kappa \sinh(\kappa(y-\eta)), \Phi) \tag{5.10}$$

$$\Theta = \Theta_1 + \mathscr{W}_{\eta}^{y}(\Theta_1, \Phi) \tag{5.11}$$

$$\Phi = \kappa^2 \eta \frac{I_1(\sqrt{\kappa^2(y^2-\eta^2)})}{\sqrt{\kappa^2(y^2-\eta^2)}} \tag{5.12}$$

$$\Theta_1 = \frac{2\mathrm{i}}{\epsilon\kappa}\eta\big(\kappa(2y-\eta-1)\sinh(\kappa(y-\eta)) - \cosh(\kappa(y-\eta)) + 1\big) \tag{5.13}$$

$$K = \kappa^2(y-\eta) + \Pi - \mathscr{W}_{\eta}^{y}(\Pi, \kappa^2(y-\eta)) \tag{5.14}$$

$$\Gamma = \Gamma_1 - \mathscr{W}_{\eta}^{y}(\Pi, \Gamma_1) \tag{5.15}$$

$$\Pi = \kappa^2 \eta \frac{J_1(\sqrt{\kappa^2(y^2-\eta^2)})}{\sqrt{\kappa^2(y^2-\eta^2)}} \tag{5.16}$$

$$\begin{aligned}\Gamma_1 = {} & \frac{\kappa \mathrm{i}}{\epsilon}\eta(y-\eta)(3y-\eta-2) \\ & -\frac{2\mathrm{i}}{3\epsilon\kappa^2}(6\kappa + 12\kappa(y-\eta) + 3\kappa^3(y-\eta)^2 - 2\kappa^3(y-\eta)^3 \\ & -6\kappa\cosh(\kappa(y-\eta)) - 24\sinh(\kappa(y-\eta)) + 12\kappa(y-\eta)\cosh(\kappa(y-\eta))),\end{aligned} \tag{5.17}$$

where $\kappa = 2\Pi k_z$, I_1 *is a modified Bessel function of the first kind and* J_1 *is a Bessel function of the first kind.*

Proof. The solutions (and their derivations) to (5.7)–(5.9) can be found in Smyshlyaev & Krstic (2004). Once Φ is found, Π is simply $-\Phi$ with κ^2 replaced with $-\kappa^2$. Also using methods from Smyshlyaev & Krstic (2004) we write L, K, Θ, Γ as

$$L = L_1 + \Phi + \mathscr{W}_{\eta}^{y}(L_1, \Phi) \tag{5.18}$$

$$K = K_1 + \Pi - \mathscr{W}_{\eta}^{y}(\Pi, K_1) \tag{5.19}$$

$$\Theta = \Theta_1 + \mathscr{W}_{\eta}^{y}(\Theta_1, \Phi) \tag{5.20}$$

$$\Gamma = \Gamma_1 - \mathscr{W}_{\eta}^{y}(\Pi, \Gamma_1), \tag{5.21}$$

where L_1, K_1, Θ_1, Γ_1 are defined by

$$\epsilon L_{1yy} = \epsilon L_{1\eta\eta} \qquad \epsilon K_{1yy} = \epsilon K_{1\eta\eta} \tag{5.22}$$

$$\epsilon L_1|_{\eta=0} = -g(y) \qquad \epsilon K_1|_{\eta=0} = \mathscr{V}(K_1, g) - g(y) \tag{5.23}$$

$$\epsilon L_1|_{\eta=y} = -g(0) \qquad \epsilon K_1|_{\eta=y} = 0 \tag{5.24}$$

$$\epsilon \Theta_{1yy} = \epsilon \Theta_{1\eta\eta} - h - \mathscr{W}_{\eta}^{y}(h, L_1) \qquad \epsilon \Gamma_{1yy} = \epsilon \Gamma_{1\eta\eta} - h \tag{5.25}$$

$$\epsilon \Theta_1|_{\eta=0} = 0 \qquad \epsilon \Gamma_1|_{\eta=0} = \mathscr{V}(\Gamma_1, g) \tag{5.26}$$

$$\epsilon \Theta_1|_{\eta=y} = 0 \qquad \epsilon \Gamma_1|_{\eta=y} = 0. \tag{5.27}$$

By inspection we find $L_1 = -g(y-\eta)/\epsilon$. By using the transformation $K_1(y,\eta) = F_K(y-\eta)$ we change the K_1 system to an integral system in F_K: $\epsilon F_K(y) = \int_0^y F_K(\eta) g(y-\eta)\mathrm{d}\eta - g(y)$. Then, by noting that $g(y)'' = k^2 g(y)$, we

https://doi.org/10.1017/S0022112009005977 Published online by Cambridge University Press

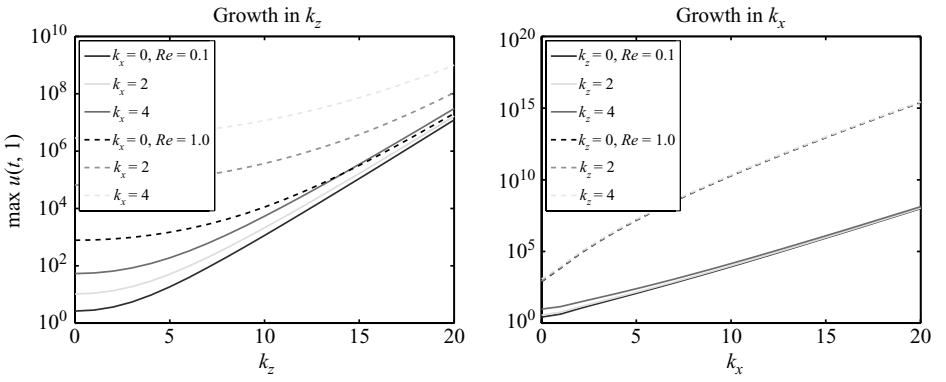


FIGURE 8. $\max_t\{|u^r|_{y=1}|\}$ growing in k_z and k_x forced by $u^r_y|_{y=0} = \sin(t)$.

can rearrange the F_K system into a solvable second-order ordinary differential equation: $F_K'' = 0$, $F_K(0) = 0$, $F_K'(0) = \kappa^2$ and find $K_1 = \kappa^2(y - \eta)$. To find Θ_1, use the change of variables $(\xi = y + \eta, \zeta = y - \eta, T(\xi, \zeta) = \Theta_1(y, \eta))$ to obtain a PDE in T: $T_{\xi\zeta} = -(1/4\epsilon)h((\xi + \zeta)/2)\cosh(\kappa\zeta)$, $T(\xi, \xi) = 0$, $T(\xi, 0) = 0$. T is then found by integrating the forcing function first with respect to ζ from zero to ζ and then with respect to ξ from ζ to ξ. Similarly, to find Γ_1, again use the change of variables $(\xi = y + \eta, \zeta = y - \eta, \Sigma(\xi, \zeta) = \Gamma_1(y, \eta))$ to obtain a PDE in Σ: $\Sigma_{\xi\zeta} = -(1/4\epsilon)h((\xi + \zeta)/2)$, $\Sigma(\xi, 0) = 0$, $\epsilon\Sigma(\xi, \xi) = \int_0^\xi \Sigma(\xi + \tau, \xi - \tau)g(\tau)\mathrm{d}\tau$. Again, integrate $\Sigma_{\xi\zeta}$ first with respect to ζ from zero to ζ and then with respect to ξ from ζ to ξ to obtain a forced integral equation for Σ. As the forcing is a function of both ξ and ζ whereas the integral part of solely a function of ζ, designate the integral part as $\Delta(\zeta)$ and find the integral equation for Δ that is only in ζ. This integral equation can then be turned into a solvable second-order ordinary differential equation by again noting that $g(y)'' = \kappa^2 g(y)$.

6. Inherent difficulty increases with Reynolds and wavenumbers

One natural question to ask of the reference solution (3.3)–(3.5) is how it grows or decays as either the wavenumbers grow or as the Reynolds number grows. We consider both cases in this section. The growth that is demonstrated in this section is inherent to the problem as the solution itself is unique and method independent. Thus large controls are primarily the result of an overly ambitious choice of reference trajectory.

The following figures examine the portion of the motion planning solution due solely to a streamwise output friction trajectory of $u^r_y|_{y=0} = \sin(t)$. They show the maximum absolute value of the input reference trajectory, $\max_t\{|u^r|_{y=1}|\}$, $\max_t\{|W^r|_{y=1}|\}$, given different system parameters when the output trajectory is as stated $(u^r_y|_{y=0} = \sin(t), W^r_y|_{y=0} = 0, p^r|_{y=0} = 0)$. Figures 8 and 9 show the growth of the input reference as the wavenumbers grow, while figure 10 demonstrates the growth as the Reynolds number grows.

The exponential growth of the motion planning solution in both wavenumber and Reynolds number is also seen when the solution is forced by only the spanwise friction output trajectory $W^r_y|_{y=0} = \sin(t)$ or by the output pressure trajectory $p^r|_{y=0} = \sin(t)$ as shown in figures 11 and 12, while figure 13 demonstrates the growth as the Reynolds number grows.

https://doi.org/10.1017/S0022112009005977 Published online by Cambridge University Press

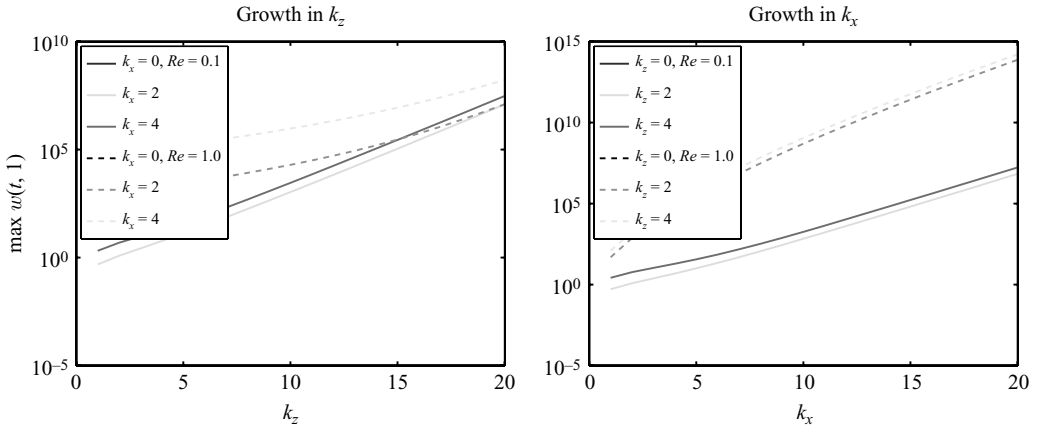


FIGURE 9. $\max_t\{|W^r|_{y=1}|\}$ growing in k_z and k_x forced by $u^r_y|_{y=0} = \sin(t)$.

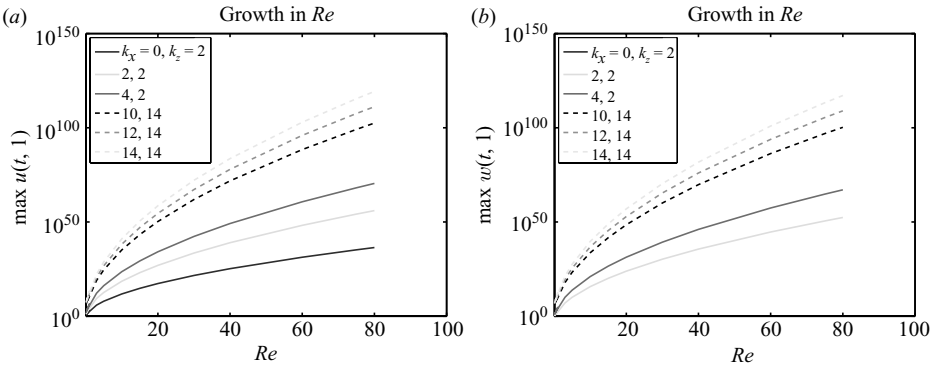


FIGURE 10. (a) $\max_t\{|u^r|_{y=1}|\}$ and (b) $\max_t\{|W^r|_{y=1}|\}$ growing in Re forced by $u^r_y|_{y=0} = \sin(t)$.

These figures show the need to carefully chose the amplitudes (and frequencies which similarly affect the growth as the Reynolds number) of the output trajectories so that the use of the inverse Fourier transform to transform the system back to physical space converges. It is important when choosing the amplitude functions to take advantage of their dependence on wavenumber as opposed to blindly choosing a constant value for all wavenumber pairs. Examples include choosing only a finite number of frequencies and choosing Gaussian functions in k_x and k_z as the amplitude functions.

It makes sense that more energy is required to generate high frequencies than low frequencies. To counter the growth due to high wavenumbers, one must decrease the amplitude at high wavenumbers. Figures 14 and 15 show how the growth changes once the amplitude of the output reference trajectory depends on wavenumber – they show the growth of the input reference due to an output reference of $p^r|_{y=0} = \mathscr{F}\{e^{-\pi^4 x^2 - \pi^4 z^2}\}\sin(t) = (1/\pi^3)e^{-(k_x^2/\pi^2 - k_z^2/\pi^2)}\sin(t)$. The dependence seen in these figures is much more acceptable.

https://doi.org/10.1017/S0022112009005977 Published online by Cambridge University Press

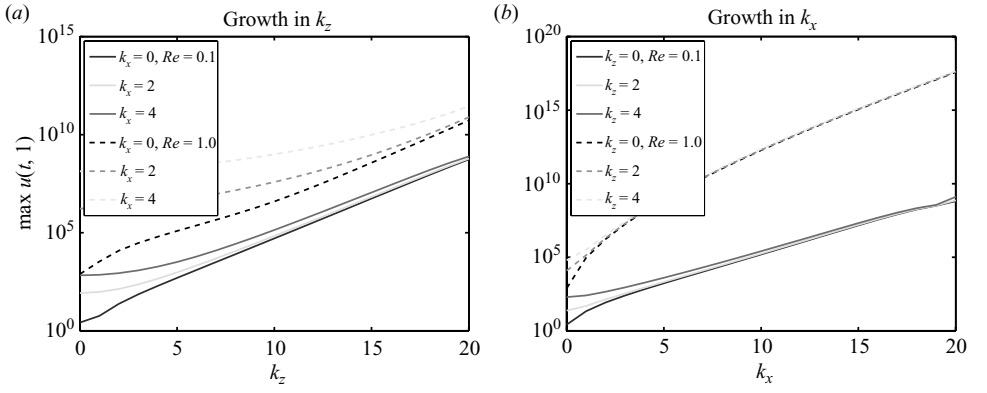


FIGURE 11. $\max_t\{|u^r|_{y=1}|\}$ growing in k_z and k_x forced by $p^r|_{y=0} = \sin(t)$.

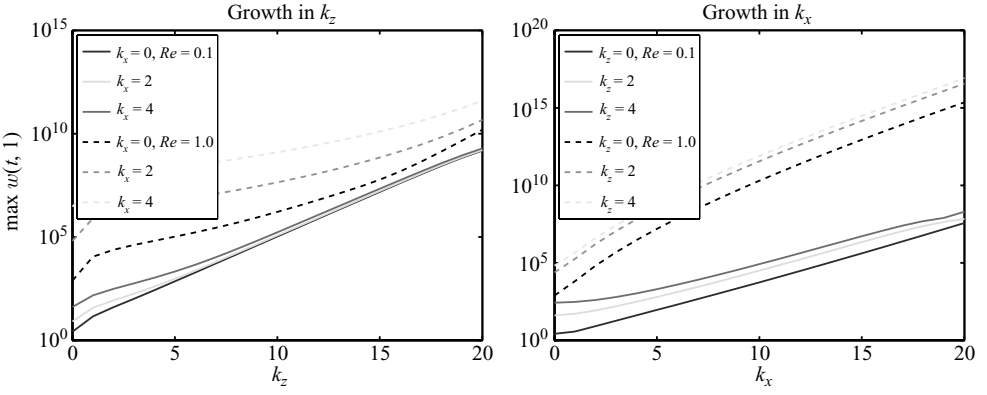


FIGURE 12. $\max_t\{|W^r|_{y=1}|\}$ growing in k_z and k_x forced by $p^r|_{y=0} = \sin(t)$.

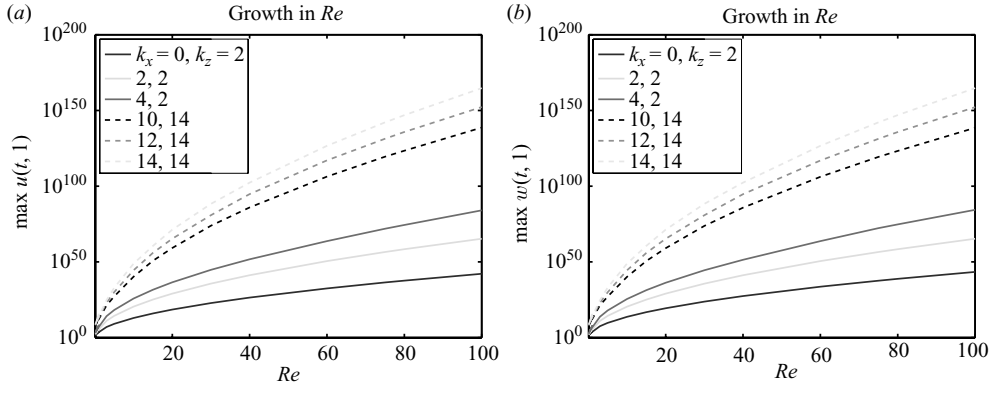


FIGURE 13. (*a*) $\max_t\{|u^r|_{y=1}|\}$ and (*b*) $\max_t\{|W^r|_{y=1}|\}$ growing in Re forced by $p^r|_{y=0} = \sin(t)$.

7. Conclusion

The PDE backstepping theory enables the synthesis of the exact solution to the motion planning problem for skin friction and pressure for the three-dimensional

https://doi.org/10.1017/S0022112009005977 Published online by Cambridge University Press

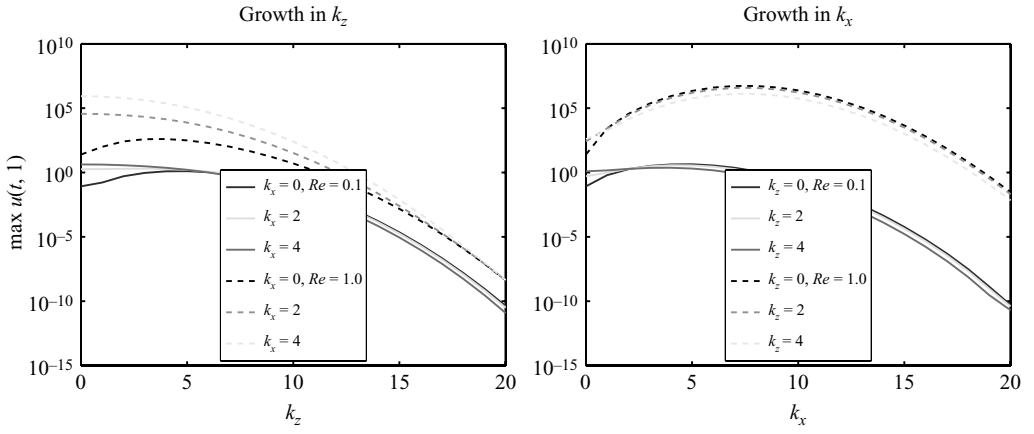


FIGURE 14. $\max_t\{|u^r|_{y=1}|\}$ growing in k_z and k_x forced by $p^r|_{y=0} = (1/\pi^3)e^{-(k_x^2/\pi^2 - k_z^2/\pi^2)}\sin(t)$.

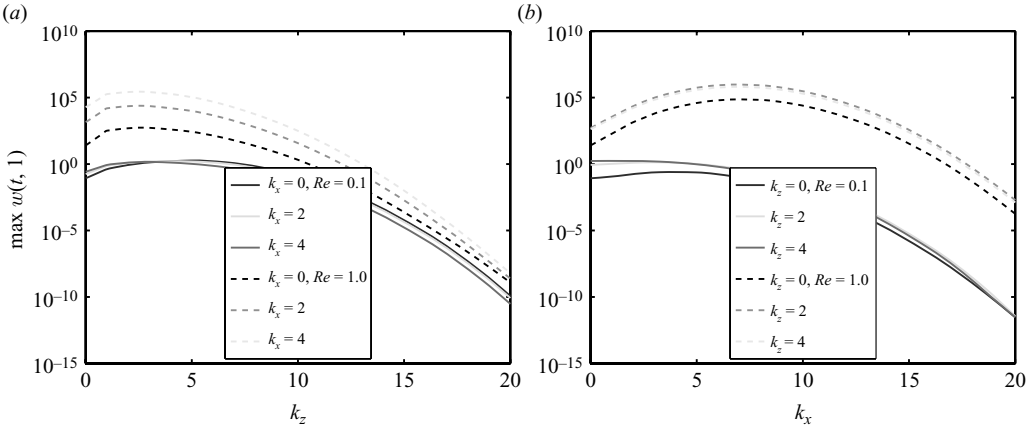


FIGURE 15. $\max_t\{|W^r|_{y=1}|\}$ growing in k_z and k_x forced by $p^r|_{y=0} = (1/\pi^3)e^{-(k_x^2/\pi^2 - k_z^2/\pi^2)}\sin(t)$.

linearized Navier–Stokes equations modelling channel flow. This is the first such result in the field of flow control. The PDE backstepping theory also allows us to stabilize the system about the reference solution, and thus achieve trajectory tracking for skin friction and pressure outputs. We hope to expand this study to state prediction and aircraft maneuverability with fluidic actuators.

The growth of the solution due to the Reynolds number serves to actually encourage us to turn to the fully nonlinear Navier–Stokes equations for motion planning purposes. As the only way to move energy in the linearized equations is through the diffusive properties tied to the Reynolds number, as the Reynolds number goes up, the energy needed to affect the far wall increases – as seen in the figures in this paper. However, the convective terms in the nonlinear equations could be useful for motion planning.

Motion planning for *boundary layer flows* is of great physical relevance. However, due to the collocated input–output structure, this system is not differentially flat and is likely to have unstable inverse dynamics at high Reynolds numbers. Future research should focus on identifying collocated flow problems that allow motion planning.

https://doi.org/10.1017/S0022112009005977 Published online by Cambridge University Press

The authors gratefully acknowledge discussions with Rafael Vazquez, Andrey Smyshlyaev and Tom Bewley. This work was supported by an NDSE Graduate fellowship and NSF.

REFERENCES

Aamo, O.-M. & Krstic, M. 2002 *Flow Control by Feedback: Stabilization and Mixing*. Springer-Verlag.

Aamo, O.-M. & Krstic, M. 2004 Feedback control of particle dispersion in bluff body wakes. *Intl J. Control* **77**, 1001–1018.

Ablowitz, M. J., Kruskal, M. D. & Ladik, J. F. 1979 Solitary wave collisions. *SIAM J. Appl. Math.* **36**, 428–437.

Baker, J. & Christofides, P. D. 2002 Drag reduction in transitional linearized channel flow using distributed control. *Intl J. Control* **75** (15), 1213–1218.

Balogh, A., Liu, W.-J. & Krstic, M. 2001 Stability enhancement by boundary control in 2D channel flow. *IEEE Trans. Automat. Control* **46**, 1696–1711.

Bamieh, B. & Dahleh, M. 2001 Energy amplification in channel flows using stochastic exictation. *Phys. Fluids* **13** (11).

Baramov, L., Tutty, O. R. & Rogers, E. 2002 Robust control of linearized Poiseuille flow. *J. Guidance Control Dyn.* **25** (1), 145–151.

Baramov, L., Tutty, O. R. & Rogers, E. 2004 H_∞ control of nonperiodic two-dimensional channel flow. *IEEE Trans. Control Syst. Technol.* **12** (1), 111–122.

Barbu, V. 2003 Feedback stabilization of Navier–Stokes equations. *ESAIM: Control, Optim. Cal. Var.* **9**, 197–205.

Bewley, T. R. 2001 Flow control: new challenges for a new renaissance. *Progress in Aerospace Sciences* **37**, 21–58.

Bewley, T. R. & Liu, S. 1998 Optimal and robust control and estimation of linear paths to transition. *J. Fluid Mech.* **365**, 305–349.

Glezer, A. & Allen, M. 2002 Micromachined synthetic jet actuators and applications thereof. U.S. Patent 5758823.

Gunzburger, M. D. & Lee, H. C. 1991 Feedback control of karman vortex shedding. *J. Appl. Mech.* **63** (3), 828–835.

Hogberg, M., Bewley, T. R. & Henningson, D. S. 2003 Linear feedback control and estimation of transition in plane channel flow. *J. Fluid Mech.* **481**, 149–175.

Ilak, M. & Rowley, C. W. 2008 Modeling of transitional channel flow using balanced proper orthogonal decomposition. *Phys. Fluids* **20**, 034103.

Isidori, A. 1995 *Nonlinear Control Systems*. Springer-Verlag.

Joshi, S. S., Speyer, J. L. & Kim, J. 1997 A systems theory approach to the feedback stabilization of infinitesimal and finite-amplitude disturbances in plane Poiseuille flow. *J. Fluid Mech.* **332**, 157–184.

Jovanovic, M. & Bamieh, B. 2005 Componentwise energy amplification in channel flows. *J. Fluid Mech.* **534**, 145–183.

Krstic, M., Cochran, J. & Vazquez, R. 2008 Backstepping controllers for stabilization of turbulent flow pdes. In *Modeling and Control of Complex Systems* (ed. P. Ioannou & I. Pitsilides). CRC Press.

Krstic, M., Kanellakopoulos, I. & Kokotovic, P. 1995 *Nonlinear and Adaptive Control Design*. John Wiley and Sons.

Laroche, B. & Martin, P. 2000 Motion planning for a 1-D diffusion equation using a Brunovsky-like decomposition. In *14th International Symposium of Mathematical Theory of Networks and Systems*. Perpignan, France.

Laroche, B., Martin, P. & Rouchon, P. 2000 Motion planning for the heat equation. *Intl J. Robust Nonlinear Control* **10**, 629–644.

Meurer, T. & Zeitz, M. 2005 Feedforward and feedback tracking control of nonlinear diffusion – convection – reaction systems using summability methods. *Indust. Engng Chem. Res.* **44** (8), 2532–2548.

https://doi.org/10.1017/S0022112009005977 Published online by Cambridge University Press

Ollivier, F. & Sedoglavic, A. 2001 A generalization of flatness to nonlinear systems of partial differential equations. Application to the command of a flexible rod. In *5th IFAC Symposium on Nonlinear Control Systems*. St Petersburg, Russia.

Protas, B. & Styczek, A. 2002 Optimal rotary control of the cylinder wake in the laminar regime. *Phys. Fluids* **14**, 2073–2087.

Raymond, J.-P. 2006 Feedback boundary stabilization of the two dimensional Navier–Stokes equations. *SIAM J. on Control Optim.* **45**, 790–828.

Rouchon, P. 2001 Motion planning, equivalence, infinite dimensional systems. *Intl J. Appl. Math. Comput. Sci.* **11** (1), 165–188.

Schmid, P. J. & Henningson, D. S. 2001 *Stability and Transition in Shear Flows*. Springer-Verlag.

Smyshlyaev, A. & Krstic, M. 2004 Closed-form boundary state feedback for a class of 1-D partial integro-differential equations. *IEEE Trans. Automat. Control* **49**, 2185–2202.

Vazquez, R., Coron, J. M. & Trelat, E. 2006*a* Stable Poiseuille flow transfer for a Navier-Stokes system. In *25th American Control Conference*.

Vazquez, R. & Krstic, M. 2007*a* A closed-form feedback controller for stabilization of the linearized 2D Navier–Stokes Poisseuille flow. *IEEE Trans. Automat. Control* **52** (12), 2298–2312. Minneapolis, MN, USA.

Vazquez, R. & Krstic, M. 2007*b* *Control of Turbulent and Magnetohydrodynamic Channel Flows*. Birkhauser. San Diego, CA, USA.

Vazquez, R., Schuster, E. & Krstic, M. 2006*b* A closed-form observer for the 3D inductionless MHD and Navier-Stokes channel flow. In *45th IEEE Conference on Decision and Control,* pp. 739–746.

Veres, S. M., Baramov, L., Tutty, O. R. & Rogers, E. 2003 Iterative design for active control of fluid flow. *Intl J. Control* **76** (14), 1375–1386.

Yuan, C. C., Krstic, M. & Bewley, T. 2004 Active control of jet mixing. *IEE Proc.: Control Theory Appl.* **151**, 763–772.

https://doi.org/10.1017/S0022112009005977 Published online by Cambridge University Press